

Orbital order and electron itinerancy in CoV_2O_4 and $\text{Mn}_{0.5}\text{Co}_{0.5}\text{V}_2\text{O}_4$ from first principles

Jyoti Krishna¹ and T. Maitra^{2,*}

¹*Department of Physics, Arizona State University, Tempe, AZ - 85287, USA*

²*Department of Physics, Indian Institute of Technology Roorkee, Roorkee 247667, Uttarakhand, India*

In view of the recent experimental predictions of a weak structural transition in CoV_2O_4 we explore the possible orbital order states in its low temperature tetragonal phases from first principles density functional theory calculations. We observe that the tetragonal phase with $I4_1/amd$ symmetry is associated with an orbital order involving complex orbitals with a reasonably large orbital moment at Vanadium sites while in the phase with $I4_1/a$ symmetry, the real orbitals with quenched orbital moment constitute the orbital order. Further, to study the competition between orbital order and electron itinerancy we considered $\text{Mn}_{0.5}\text{Co}_{0.5}\text{V}_2\text{O}_4$ as one of the parent compounds, CoV_2O_4 , lies near itinerant limit while the other, MnV_2O_4 , lies deep inside the orbitally ordered insulating regime. Orbital order and electron transport have been investigated using first principles density functional theory and Boltzmann transport theory in CoV_2O_4 , MnV_2O_4 and $\text{Mn}_{0.5}\text{Co}_{0.5}\text{V}_2\text{O}_4$. Our results show that as we go from MnV_2O_4 to CoV_2O_4 there is enhancement in the electron's itinerancy while the nature of orbital order remains unchanged.

I. INTRODUCTION

The family of spinel vanadates AV_2O_4 (AVO) presents a perfect platform for understanding the interplay among all possible degrees of freedom in a solid such as spin, orbital, lattice and charge^{1,2}. In addition, the Mott physics is also at play here, as by mere controlling of the V-V distance (by varying the size of A^{2+} ion), the system can be driven to its itinerant state from an orbitally and magnetically ordered insulating state^{3,4}. One can thus observe a fascinating competition between orbital order and electron itinerancy by tuning V-V distance in these materials. An additional geometrical frustration due to pyrochlore lattice of V^{3+} ions, makes spinel vanadates a fertile ground to study competing magnetic interactions (J_{V-V} and J_{A-V}) on a geometrically frustrated lattice. Whilst, the partially filled t_{2g} orbitals of V^{3+} ions, makes it always orbitally active, thereby triggering a structural transition, a magnetic transition normally follows at low temperatures due to the partial lifting of geometrical frustration. The multiple transitions (structural and magnetic) in AVO is thus a consequence of the nature of A^{2+} ion being magnetic, orbitally active or both (e.g. MnV_2O_4 , CoV_2O_4 , FeV_2O_4 etc.)⁵⁻⁸.

Among the spinel vanadates with magnetic A-site ion, CoV_2O_4 is unique in two ways: one, it sits very close to itinerancy limit 2.94 \AA in terms of V-V distance (R_{V-V})⁸⁻¹⁰ such that on the application of moderate pressure (about $\sim 8 \text{ GPa}$) it shows metallic behavior¹¹ and two, the existence of any structural transition in this compound is highly debated with most of the earlier experimental reports finding no evidence of cubic to tetragonal structural transition in this system^{8,11,12} whereas recent reports claim to observe a weak structural transition^{10,13}. Interestingly though, it has got the highest magnetic transition temperatures: a collinear ferrimagnetic transition temperature $T_C = 150 \text{ K}$ and

a non-collinear ferrimagnetic $T_{NC} = 90 \text{ K}$ ¹³ among the AVOs. Recent strain measurements have reportedly identified a weak first order structural transition ($\Delta a/a \sim 10^{-4}$) at 90 K concurrent with T_{NC} ^{10,13}. Further, from the dielectric measurements, the authors proposed an orbital glassy state to be present at low temperatures. From another recent high resolution neutron powder diffraction measurement a very small tetragonal distortion ($1 - c/a < 0.06\%$) has been captured in CoV_2O_4 at 95 K and on further lowering of temperature, a change in the tetragonal symmetry from $I4_1/amd$ to $I4_1/a$ was observed at 59 K via single crystal synchrotron radiation measurement¹⁴. Further analysis has led the authors to propose an anti-ferro orbitally ordered state below 59 K .

MnV_2O_4 , on the other hand, is insulating in character and R_{V-V} is away from the itinerancy limit and orbitally ordered^{5,15-20}. Here, competing superexchange interactions J_{Mn-V} and J_{V-V} lead to two magnetic transitions: a collinear ferrimagnetic transition (T_C) at 56 K (V spins aligned opposite to that of Mn spins along c-direction) and a non-collinear ferrimagnetic (T_{NC}) transition (V spins cant away from c-axis while Mn spins remain parallel to c-axis) at 53 K . Also, the structural transition (cubic to tetragonal with space group $I4_1/a$) is well established in this system which occurs at 53 K coincident with T_{NC} . In the tetragonal phase, VO_6 octahedra are compressed along c-axis because of Jahn-Teller (JT) effect. The tetragonal compression along c-axis lowers the d_{xy} orbital which then gets occupied by one electron. The second electron has therefore the choice of going to either d_{xz} , d_{yz} or both paving the way for a possible orbital ordering in the system. The cooperative JT effect forces the orbitals to order in certain fashion relieving the frustration of the lattice.

Many theoretical models are proposed for orbital order (OO) in spinel vanadates that depends on the relative strength of SO coupling, superexchange and

JT interaction^{21–23}. The possible scenarios for OO in these systems are (1) A-type anti-ferro (real) OO, in which the second electron of V ion, alternately occupies d_{xz}/d_{yz} orbital in successive ab-planes along c direction resulting in the quenching of orbital angular momentum L, (2) Ferro (complex) OO, results in the ordering of complex orbitals ($d_{yz} \pm i d_{xz}$) due to enhanced SO coupling leading to unquenched L. X-ray Magnetic Circular Dichroism (XMCD) technique has been very useful for detecting the local orbital moment^{24,25} which provides the information about real or complex orbital ordering. In case of MnV_2O_4 , previous DFT calculations indicate real orbital ordering^{26,27} which was corroborated by XMCD measurements²⁴.

In a recent measurement, Ma et al.²⁸ have looked into the effect of Co doping in MnV_2O_4 and observed a crossover from orbitally ordered low Co-doping regime to increased electron itinerancy in high Co-doped regime. Therefore, it would be interesting to explore using first principles DFT and transport calculations the following two phenomena. Firstly, the nature of orbital ordering in low temperature phases of CoV_2O_4 in view of the structural transitions observed recently in experiments¹⁴ and secondly, the competition between orbital order and electron itinerancy as a function of Co doping as we go from MnV_2O_4 to CoV_2O_4 . We have addressed above two issues in our work presented in this paper.

II. METHODOLOGY

The first principles density functional theory and Boltzmann transport theory have been used for the calculations presented in this paper. The structural parameters for MnV_2O_4 and CoV_2O_4 (in its different structural phases) were obtained from experiments^{14,15}. For $\text{Mn}_{0.5}\text{Co}_{0.5}\text{V}_2\text{O}_4$, 50% of Mn ions were substituted by Co in the experimental structure of the MnV_2O_4 . We have then optimized both parent (MnV_2O_4 and CoV_2O_4) and doped structures using 2Doptimize package available in WIEN2k²⁹. This package effectively performs 2D optimization in volume, c/a and atomic positions. The optimization (volume, c/a and oxygen positions) were carried out within Perdew-Burke-Ernzerhof Generalized Gradient Approximation (PBE-GGA)³⁰ exchange-correlation functional within the full potential linearized augmented plane wave (FP-LAPW) method as implemented in WIEN2k. In this, we have considered nine different structures having their volumes varied by 0.5%, 1.0%, 1.5% and 2.0% with respect to experimental structure, and for each volume, nine different c/a structures were taken. We obtained the minimum energy structure from a total 81 different structures where oxygen positions were allowed to relax. Using this optimized structure, we performed further self-consistent field calculations considering 78 \vec{k} points in the irreducible Brillouin zone and plane wave cut off ($R_{mt}K_{max}$) to be

TABLE I. The V-O bond lengths in the ab-plane and along c, A-O bond length for $x=0.0$ (MnV_2O_4), $x=0.5$ ($\text{Mn}_x\text{Co}_{1-x}\text{V}_2\text{O}_4$) and $x=1.0$ (CoV_2O_4) after structural optimization.

| x | V-O (c) | V-O (ab) | A-O |
|--------------------------|---------|-----------------|--------|
| 0.0 | 2.0293 | (2.0434,2.0137) | 2.0346 |
| 0.5 | 2.0191 | (2.0331,2.0036) | 2.0244 |
| 1.0 | | | |
| <i>Fd3m</i> (PHASE 1) | 2.0169 | (2.0169,2.0169) | |
| <i>I41/amd</i> (PHASE 2) | 2.0148 | (2.0176,2.0176) | |
| <i>I41/a</i> (PHASE 3) | 2.0150 | (2.0059,2.0295) | 1.9696 |

8.0. The muffin tin radii were taken as 2.0, 1.95 and 1.65 a.u. for Mn/Co, V and O respectively. Due to the presence of 3d electrons, Coulomb correlation (U) becomes indispensable, which was included in our calculations within GGA+U³¹. This takes into account the on-site Coulomb interaction and removes the self Coulomb and self exchange-correlation energy. The spin-orbit coupling (SO) is included by the second variational method with scalar relativistic wavefunctions³². To analyse the orbital order and electron transport we used maximally-localized Wannier functions (MLWF) to fit the DFT bands calculated by WIEN2k. WANNIER90³³ and WIEN2WANNIER³⁴ codes were used for this purpose. We calculated the transport properties using BoltzWann code that utilizes semi-classical Boltzmann transport theory³⁵.

III. RESULTS AND DISCUSSIONS

In view of recent experimental report¹⁴ on the observation of weak structural transitions in CoV_2O_4 from cubic ($Fd\bar{3}m$) to tetragonal ($I4_1/amd$ and $I4_1/a$) phases, we investigated the electronic structure and nature of orbital ordering in the experimentally observed tetragonal phases in this system from first principles calculations. Further, we also looked into the effect of Co doping on the competition between orbital ordering and electron itinerancy as we go from MnV_2O_4 to CoV_2O_4 . The results presented in this section have therefore been divided into two parts. In part A, we present our calculations and results on the electronic structure and orbital order analysis of the cubic ($Fd\bar{3}m$) and tetragonal ($I4_1/amd$ and $I4_1/a$) phases of CoV_2O_4 . In part B, we present our results on the effect of Co doping (x) on MnV_2O_4 where we have discussed electronic structure, orbital ordering and electron transport calculations for the parent and doped compounds. Electronic structure calculations are performed within GGA+U and GGA+U+SO approximations with $U_{eff} = U - J = 4$ eV for Mn/Co and 3 eV for V ions where U is the Coulomb correlation and J is Hund's coupling.

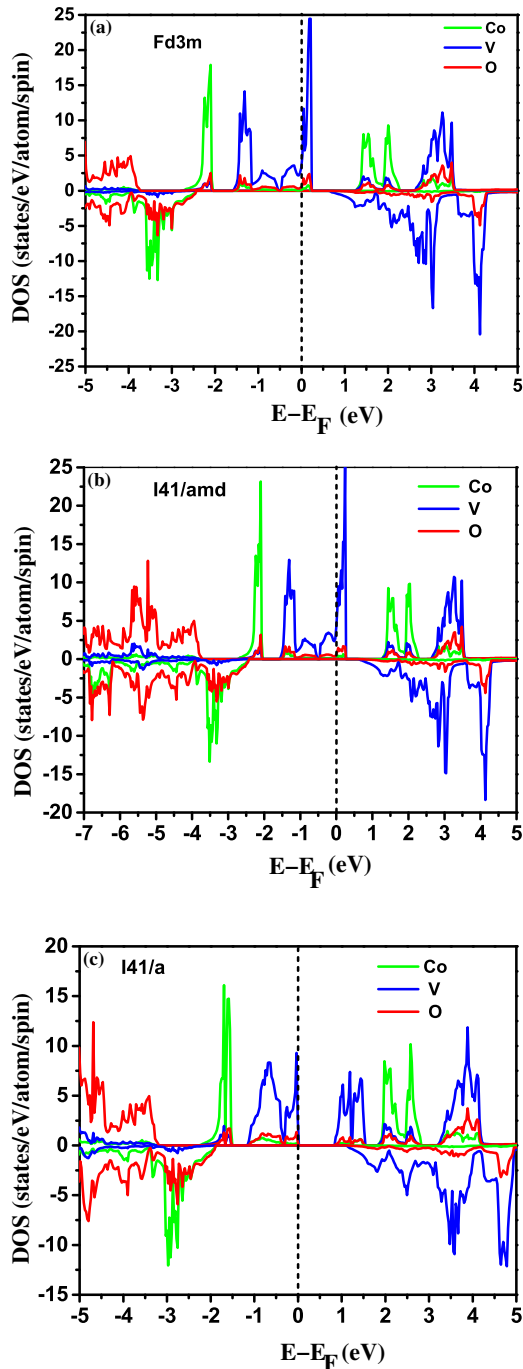


FIG. 1. The total density of states (DOS) for Co, V, and O within GGA+U for (a) cubic $Fd\bar{3}m$, (b) tetragonal $I4_1/amd$ and (c) $I4_1/a$ phases in majority and minority spin channel.

A. CoV_2O_4 and its different phases

The GGA+U calculations were carried out on the optimized structures (see Table I) for all the three structural phases (cubic (phase 1), tetragonal $I4_1/amd$ (phase 2) and tetragonal $I4_1/a$ (phase 3)) by considering a collinear

ferrimagnetic spin configuration where the spins of V are antiparallel with respect to Co spins along c -axis. The total energy calculations reveal that the tetragonal phase with $I4_1/a$ symmetry has the lowest energy which is consistent with the experiment. In Figure 1 we present the total density of states (DOS) of all the three phases of CoV_2O_4 for both the spin channels calculated within GGA+U approximation. While the cubic and tetragonal ($I4_1/amd$) phase display the metallic character even with large U (in contrary to the experiments), an insulating behavior is observed for tetragonal phase 3 ($I4_1/a$) (consistent with experiments). From DOS one can clearly observe that the tetrahedral crystal field splits the d -states of Co^{2+} ions into the lower energy e_g and higher energy t_{2g} states. Four out of the seven valence electrons of Co^{2+} thus completely fill the e_g states (both majority and minority) and the rest three electrons make t_{2g} states half-filled (only majority states are filled, minority states remain empty). Because of this, the filled Co d -states lie much below the Fermi level (FL). On the other hand, V^{3+} ions are octahedrally coordinated by O ions thus the d -states here split into higher energy e_g and lower t_{2g} states. The two d -electrons of V^{3+} ions thus partially fill the t_{2g} states that lie near Fermi level (FL). Tetragonal distortions present in phase 2 does not split the t_{2g} states completely to open a gap while in phase 3 a finite gap is seen in DOS due to the splitting of t_{2g} states (see Figure 2 below). Note that in addition to octahedral crystal field, the trigonal distortion is also present in case of V ions (as O-V-O angles deviate from 90°). Because of varying strengths of tetragonal and trigonal distortions present in three phases the nature and magnitude of splitting of t_{2g} states are different.

We present in Figure 2, the partial V DOS of three different phases calculated within GGA+U (left panel) and GGA+U+SO (right panel). One can see from Figure 2 (left) that in phase 1 (the cubic phase) where only trigonal distortion is present, the t_{2g} states split into a lower singlet a_{1g} and the higher doublet e'_g states which are linear combinations of d_{xy} , d_{xz} and d_{yz} orbitals. In phase 2, the presence of both tetragonal and the trigonal distortion create much complicated splitting of t_{2g} states. In phase 3, the extent of trigonal distortion is much lower than the tetragonal compression thus t_{2g} split into pure d_{xy} , d_{xz} and d_{yz} states. In phase 1 and 2, the highest occupied t_{2g} level remains doubly degenerate and filled by one electron and hence the system shows metallic behavior. In phase 3, however, we see a further splitting of the t_{2g} levels giving rise to a band gap in the DOS as seen in Figure 2(c)(left). This splitting is because of the Jahn-Teller (JT) distortion associated with $I4_1/a$ symmetry where the V-O bonds are different in all three directions. This is also associated with a long range orbital ordering (OO) as discussed below. Comparing the DOS of GGA+U and GGA+U+SO we observe that for phase 1 and 2 they are drastically different whereas for phase 3 they are very similar. In phase 1 and 2 we obtain an insulating electronic structure within GGA+U+SO, un-

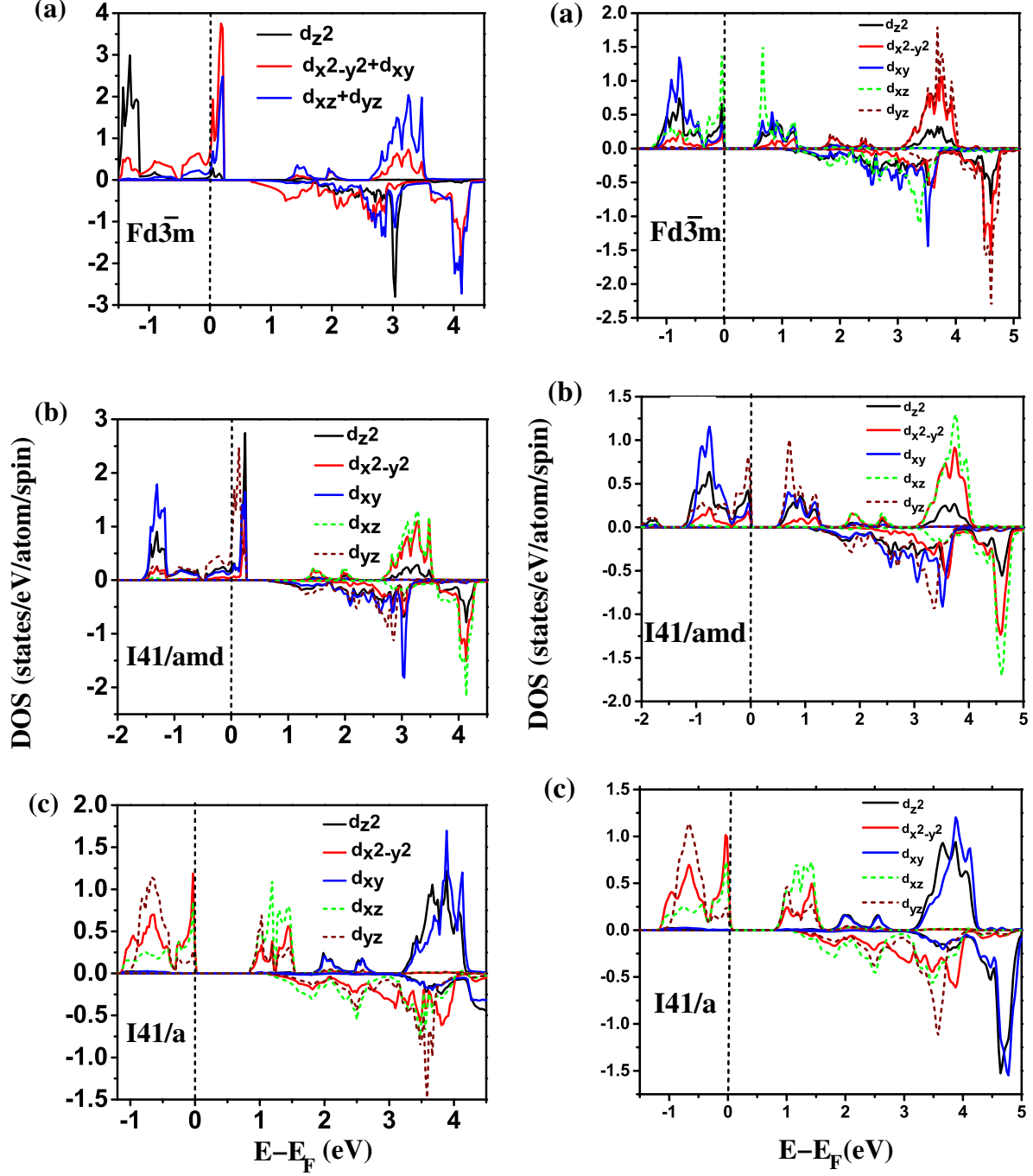


FIG. 2. The Vanadium partial density of states (DOS) for d -electrons within GGA+U (left) and for GGA+U+SO (right) for (a) cubic $Fd\bar{3}m$, (b) tetragonal $I41/amd$ and (c) $I41/a$ phases for majority and minority spin channels. Note that the set $[d_{x^2-y^2}, d_{xz}$ and $d_{yz}]$ form t_{2g} rather than conventionally used $[d_{xy}, d_{xz}$ and $d_{yz}]$ as the crystallographic a and b -axes are rotated by 45° with respect to planar V-O bonds of VO_6 octahedra.

like the metallic solution of GGA+U, which is consistent with experiment. The SO effect on DOS is seen to be quite significant in phase 1 and 2, whereas in phase 3 it is negligible. This is also reflected in calculated orbital moment values at V site which are $-0.66 \mu_B$ and $-0.06 \mu_B$ for phase 2 and 3 respectively.

In order to understand the nature of OO, which is difficult to ascertain from the DOS, we have calculated 3D electron and hole densities in real space at V sites and have also done an analysis using tight-binding (Wannier orbitals) basis for phase 2 and 3. In Figure 3 we show the calculated 3D hole densities for phase 2 and phase 3

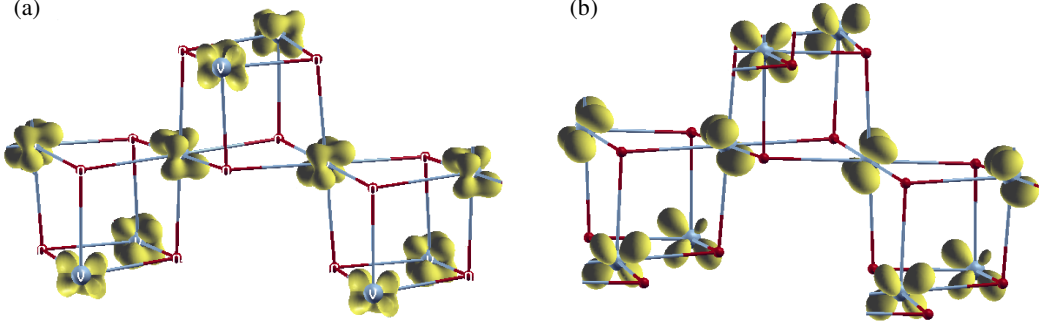


FIG. 3. 3D hole density in real space depicting the nature of unoccupied orbitals of V^{3+} ion for (a) phase 2 and (b) phase 3. The rotation of the orbitals (in ab plane and c -direction) in the V chain is because of the trigonal distortion.

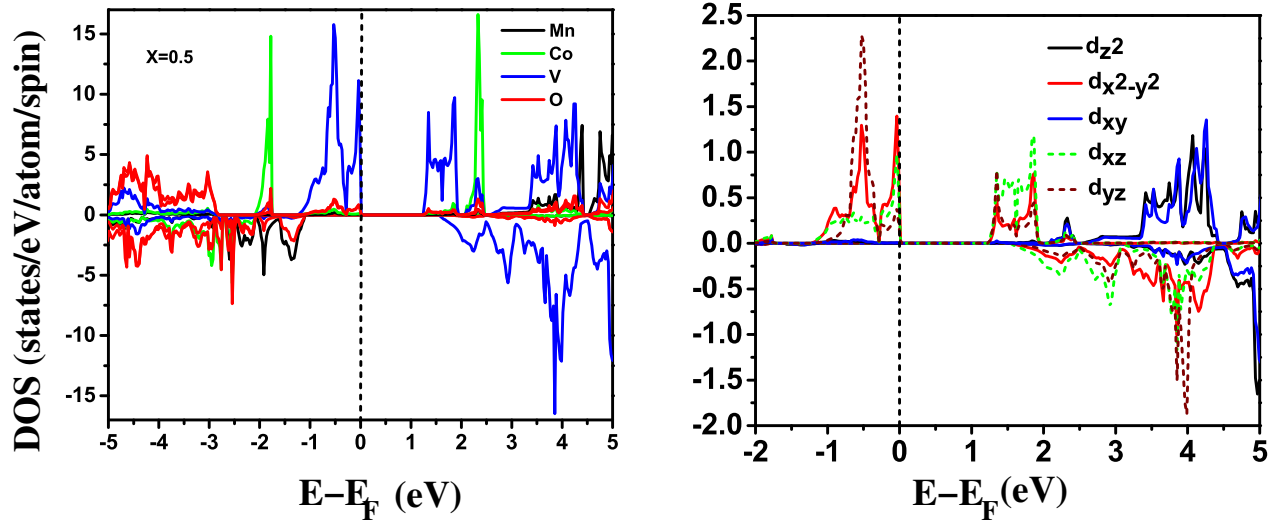


FIG. 4. *Left*: The spin-polarized total DOS for 50% ($x=0.5$) Co doping at MnV_2O_4 site calculated within GGA+U approximation. *Right*: The vanadium partial DOS for d states.

at V sites within GGA+U+SO approximation. Comparing these two one can clearly see that the unoccupied V orbital structure and hence the occupied ones are very different in phase 2 and 3. As also evident from the large orbital moment ($-0.66\mu_B$) value in case of phase 2, we propose the presence of a complex orbital order of the type $d_{xz} \pm id_{yz}$ in this case as seen in ZnV_2O_4 ²³. While in phase 3, a further analysis using Wannier orbitals basis along with a small value of calculated orbital moment ($-0.06\mu_B$) support A-type orbital order where real orbitals d_{yz} and d_{xz} are occupied at V sites in successive ab planes along c -direction. Therefore, we conclude that the transition seen in experiment¹⁴ at 59K where the crystalline symmetry changes from $I4_1/amd$ to $I4_1/a$ is also associated with complex to real orbital order transition. Future XMCD measurements are expected to shed further light on this.

B. 50% Co doped MnV_2O_4

As discussed in the introduction, MnV_2O_4 is known to be orbitally ordered while CoV_2O_4 is close to the itinerant regime. In view of the recent experimental measurements by Ma et al.²⁸ and to study the competition between electron itinerancy and orbital order in Co doped MnV_2O_4 from theoretical perspective, we considered 50% of Mn by Co in MnV_2O_4 (i.e. $Mn_{1-x}Co_xV_2O_4$ with $x=0.5$). In a previous study we have reported the effect of Co doping on the structural parameters such as lattice constants, inter-vanadium distance (R_{V-V}) etc.³⁶. With increase in Co doping at Mn sites the lattice constants a and c are seen to decrease. This is because of the smaller size of Co ion compared to that of Mn. This induced chemical pressure due to Co doping also affects R_{V-V} . We also observe that with Co doping, the Mn-O bond lengths along c -axis decrease due to the hydrostatic

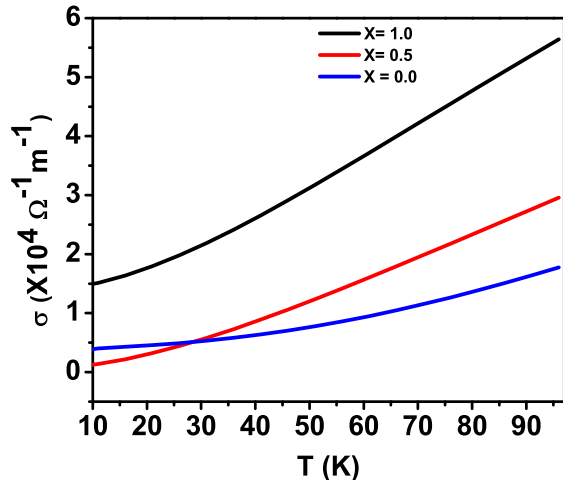


FIG. 5. The temperature dependence of electrical conductivity (σ) for different doping concentrations (x) in $\text{Mn}_{1-x}\text{Co}_x\text{V}_2\text{O}_4$.

pressure acting at Mn site which shrinks Mn-O tetrahedron (see Table I). This contraction enhances local trigonal distortion in VO_6 octahedron.

In Figure 4 we present the total and V partial DOS of $\text{Mn}_{0.5}\text{Co}_{0.5}\text{V}_2\text{O}_4$ within GGA+U approximation. Comparing the DOS for this doped compound with the same for parent compounds CoV_2O_4 (phase 3, see Figure 2) and MnV_2O_4 (not shown here), we observe that the bandgap decreases. To clearly establish that the electron itinerancy indeed increases with Co doping we have calculated the electrical conductivity as a function of temperature using Boltzmann transport theory. For this we have used Wannier fits to DFT bands of V t_{2g} states around FL obtained from Wien2k within GGA+U. The variation of electrical conductivity (σ) with temperature for MnV_2O_4 ($x=0.0$), CoV_2O_4 ($x=1.0$) and 50% Co doped ($x=0.5$) MnV_2O_4 are shown in Figure 5. We can clearly see that σ rises as Co concentration increasing indicating an enhancement of electron itinerancy in the system. Also, we see that with increasing temperature σ rises in all three cases showing the insulating character of the systems.

To ascertain how much orbital order is affected by Co doping, we have performed Wannier analysis of the V t_{2g} bands around the FL of CoV_2O_4 , MnV_2O_4 and $x = 0.5$ Co doped case. The comparison is presented in Figure 6. The projections of individual Wannier d orbitals on to V d-bands of the respective compounds are shown. The color code depicts the strength of the orbital character with red representing the highest. One can clearly see that in all three cases d_{xy} orbital is predominantly occupied at a V site whereas there is a difference between occupancies of d_{xz} and d_{yz} orbitals. Further analysis by plotting these Wannier orbitals in real space reveals that

A-type OO similar to phase 3 of CoV_2O_4 prevails in all three compounds (i.e. one electron of V^{3+} always occupies at d_{xy} orbital with another electron alternating between d_{xz} and d_{yz}). If we consider the difference between the orbital occupancies of d_{xz} and d_{yz} orbitals as the strength of the orbital order, then one can clearly see from Figure 6 that in MnV_2O_4 and $x = 0.5$ Co doped case this difference is somewhat larger than the same in CoV_2O_4 . Thus one can conclude from the above discussion that as we go from MnV_2O_4 to CoV_2O_4 , the electron itinerancy increases, the nature of orbital order remains same while the strength of orbital order weakens. Finally we would like to mention that we have also performed calculations including SO interaction for the doped compound to see whether complex orbitals are present in this case. The orbital moment for V ion is found to be $-0.068 \mu_B$ which is very small. Thus here also only real orbitals are involved in OO.

IV. CONCLUSIONS

We have performed the first principles calculation in the three different structural phases of CoV_2O_4 : cubic, tetragonal with $I4_1/\text{amd}$ symmetry and tetragonal with $I4_1/a$ symmetry. Total energy calculations reveal that tetragonal with $I4_1/a$ symmetry is indeed lower in energy with respect to the cubic phase. Our GGA+U calculations show that while cubic and tetragonal phase with $I4_1/\text{amd}$ symmetry remain metallic in character, the tetragonal phase with $I4_1/a$ symmetry becomes insulating. We observe further from our GGA+U+SO calculations that tetragonal phase with $I4_1/\text{amd}$ symmetry has orbital order involving complex orbitals with large orbital moment whereas tetragonal phase with $I4_1/a$ symmetry has A-type orbital order comprising of real orbitals with negligible orbital moment. Therefore, we conclude that the structural transition seen in experiment at 59K where the symmetry of tetragonal phase changes from $I4_1/\text{amd}$ to $I4_1/a$, is associated with complex to real orbital order transition. We also performed calculations for 50% Co doped MnV_2O_4 compound (i.e. $\text{Mn}_{0.5}\text{Co}_{0.5}\text{V}_2\text{O}_4$) to study the competition between electron itinerancy and orbital order as a function of doping. We observed that doping Co at Mn sites indeed reduces the strength of orbital order even though the orbital order remains the same. At the same time, it enhances the electron itinerancy which we could clearly see from calculated electrical conductivity which increases with the Co content.

V. ACKNOWLEDGEMENT

This work is supported by DST-DAAD project (grant no INT/FRG/DAAD/P-16/2018). JK acknowledges MHRD(INDIA) for research fellowship.

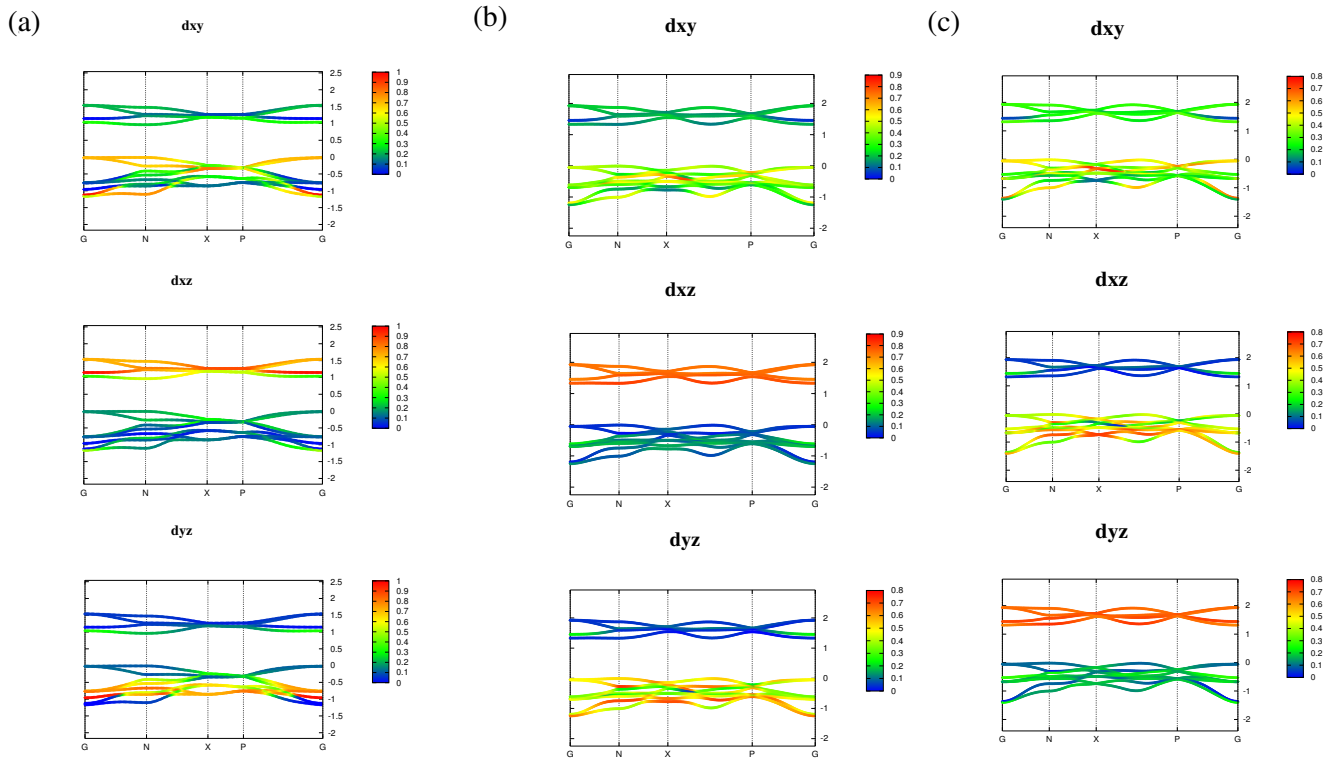


FIG. 6. Projection of V t_{2g} bands on to d_{xy} , d_{xz} and d_{yz} Wannier orbitals for (a) CoV_2O_4 in phase 3 (b) MnV_2O_4 and (c) $x=0.5$. The color bar on right side depicts the orbital character with the red (blue) color showing highest (lowest) character of a particular orbital.

* tulimfph@iitr.ac.in

¹ Paolo G Radaelli, New Journal of Physics **7**, 53 (2005).

² S.-H. Lee, H. Takagi, D. Louca, M. Matsuda, S. Ji, H. Ueda, Y. Ueda, T. Katsufuji, J.-H. Chung, S. Park, S.-W. Cheong, and C. Broholm, Journal of the Physical Society of Japan **79**, 011004 (2010).

³ A. Kiswandhi, J. Ma, J. S. Brooks, and H. D. Zhou, Physical Review B **90**, 155132 (2014).

⁴ A. Kiswandhi, J. S. Brooks, J. Lu, J. Whalen, T. Siegrist, and H. D. Zhou, Phys. Rev. B **84**, 205138 (2011).

⁵ V. O. Garlea, R. Jin, D. Mandrus, B. Roessli, Q. Huang, M. Miller, A. J. Schultz, and S. E. Nagler, Physical Review Letters **100**, 066404 (2008).

⁶ S. Kawaguchi, H. Ishibashi, S. Nishihara, M. Miyagawa, K. Inoue, S. Mori, and Y. Kubota, Journal of Physics: Condensed Matter **25**, 416005 (2013).

⁷ S. Kawaguchi, H. Ishibashi, S. Nishihara, S. Mori, J. Campo, F. Porcher, O. Fabelo, K. Sugimoto, J. Kim, K. Kato, M. Takata, H. Nakao, and Y. Kubota, Physical Review B **93**, 024108 (2016).

⁸ Y. Huang, Z. Yang, and Y. Zhang, Journal of Physics: Condensed Matter **93**, 056003 (2012).

⁹ R. Kaur, T. Maitra, and T. Nautiyal, Journal of Physics: Condensed Matter **26**, 045505 (2014).

¹⁰ Reig-i-Plessis, D. Casavant, V. O. Garlea, A. A. Aczel, M. Feyngenson, J. Neufeind, H. D. Zhou, S. E. Nagler, and G. J. MacDougall, Physical Review B **93**, 014437 (2016)

¹¹ A. Kismarhardja, J. S. Brooks, A. Kiswandhi, K. Matsubayashi, R. Yamanaka, Y. Uwatoko, J. Whalen, T. Siegrist and H. D. Zhou, Physical Review Letters **106**, 056602(4) (2011).

¹² J. H. Lee, J. Ma, S. E. Hahn, H. B. Cao, M. Lee, T. Hong, H.-J. Lee, M. S. Yeom, S. Okamoto, H. D. Zhou, M. Matsuda and R. S. Fishman, Scientific Reports **7**, 17129 (2017).

¹³ R. Koborinai, S. E. Dissanayake, M. Reehuis, M. Matsuda, T. Kajita, H. Kuwahara, S.- H. Lee, and T. Katsufuji, Physical Review Letters **116**, 037201 (2016).

¹⁴ H. Ishibashi, S. Shimono, K. Tomiyasu, S. Lee, S. Kawaguchi, H. Iwane, H. Nakao, S. Torii, T. Kamiyama, and Y. Kubota, Physical Review B **96**, 144424 (2017).

¹⁵ Y. Nii, H. Sagayama, T. Arima, S. Aoyagi, R. Sakai, S. Maki, E. Nishibori, H. Sawa, K. Sugimoto, H. Ohsumi, and M. Takata, Physical Review B **86**, 125142 (2012).

¹⁶ S.- H. Baek, N. J. Curro, K.- Y. Choi, A.P. Reyes, P.L. Kuhns, H. D. Zhou, and C. R. Wiebe, Physical Review B **80**, 140406(R) (2009).

¹⁷ J.- H. Chung, J.- H. Kim, S.- h. Lee, T. J. Sato, T. Suzuki, M. Katsumura, and T. Katsufuji, Physical Review B **77**,

- 054412 (2008).
- ¹⁸ H. D. Zhou, J. Lu, and C. R. Weibe, *Physical Review B* **76**, 174403 (2007).
 - ¹⁹ K. Adachi, T. Suzuki, K. Kato, K. Osaka, M. Takata, and T. Katsufuji, *Physical Review Letters* **95**, 197202 (2005).
 - ²⁰ T. Suzuki, M. Katsumura, K. Taniguchi, T. Arima, and T. Katsufuji, *Physical Review Letters* **98**, 127203 (2007).
 - ²¹ H. Tsunetsugu, Y. Motome, *Physical Review B* **68**, 060405(R)(2003).
 - ²² O. Tchernyshyov, *Physical Review Letters* **93**, 15 (2004).
 - ²³ T. Maitra, and R. Valenti, *Physical Review Letters* **99**, 126401 (2007).
 - ²⁴ K. Matsuura, H. Sagayama, Y. Nii, N. D. Khanh, N. Abe, and T. Arima, *Physical Review B* **92**, 035133 (2015).
 - ²⁵ J. Okabayashi, S. Miyasaka, K. Hemmi, K. Tanaka, S. Tajima, H. Wadati, A. Tanaka, Y. Takagi, and T. Yokoyama, *Journal of the Physical Society of Japan* **84**, 104703 (2015).
 - ²⁶ S. Sarkar, T. Maitra, R. Valenti, and T. Saha-Dasgupta, *Physical Review Letters* **102**, 216405 (2009).
 - ²⁷ D. Dey, T. Maitra and A. Taraphder, *Physical Review B* **93**, 195133 (2016).
 - ²⁸ J. Ma, J. H. Lee, S. H. Hahn, T. Hong, H. B. Cao, A. A. Aczel, Z. L. Dun, M. B. Stone, W. Tian, Y. Qiu, J. R. D. Copley, H. D. Zhou, R. S. Fishman, and M. Matsuda, *Physical Review B* **91**, 020407(R) (2015).
 - ²⁹ P. Blaha, K. Schwarz, G. K. H. Madsen, D. Kvasnicka, and J. Luitz, *WIEN2k An Augmented Plane Wave + Local Orbitals Program for Calculating Crystal Properties* (Karlheinz Schwarz, Techn. Universität Wien, Austria, 2001).
 - ³⁰ J. P. Perdew, A. Ruzsinszky, G. I. Csonka, O. A. Vydrov, G. E. Scuseria, L. A. Constantin, X. Zhou, and K. Burke, *Physical Review Letters* **100**, 136406 (2008).
 - ³¹ V. I. Anisimov, I. V. Solovyev, and M. A. Korotin, *Physical Review B* **48**, 23 (1993).
 - ³² D. D. Koelling, and B. N. Harmon, *Journal of Physics C: Solid State Physics* **10**, 3107 (1977).
 - ³³ A. A. Mostofi, J. R. Yates, Y.-S. Lee, I. Souza, D. Vanderbilt, and N. Marzari, *Computer Physics Communications* **178**, 685 (2008).
 - ³⁴ J. Kunes, R. Arita, P. Wissgott, A. Toschi, H. Ikeda, K. Held, *Computer Physics Communications* **181**, 1888 (2010).
 - ³⁵ G. Pizzi, D. Volja, B. Kozinsky, M. Fornari, and N. Marzari, *Computer Physics Communications* **185**, 422 (2014).
 - ³⁶ Jyoti Krishna and Tulika Maitra, *AIP Conference Proceedings* **1832**, 090022 (2017).